An electrical analysis of slow wave propagation in the guinea-pig gastric antrum

Frank R. Edwards and G. David S. Hirst

Division of Neuroscience, John Curtin School of Medical Research, Canberra, ACT, 0200, Australia

This paper provides an electrical description of the propagation of slow waves and pacemaker potentials in the guinea-pig gastric antrum in anal and circumferential directions. As electrical conduction between laterally adjacent circular muscle bundles is regularly interrupted, anal conduction of pacemaker potentials was assumed to occur via an electrically interconnected chain of myenteric interstitial cells of Cajal (ICC_{MY}). ICC_{MY} were also connected resistively to serially connected compartments of longitudinal muscle. Circumferential conduction occurred in a circular smooth muscle bundle that was represented as a chain of electrically connected isopotential compartments: each compartment contained a proportion of intramuscular interstitial cells of Cajal (ICC_{IM}) that are responsible for the regenerative component of the slow wave. The circular muscle layer, which contains ICC_{IM}, and the ICC_{MY} network incorporated a mechanism, modelled as a two-stage chemical reaction, which produces an intracellular messenger. The first stage of the reaction is proposed to be activated in a voltage-dependent manner as described by Hodgkin and Huxley; the messenger altered the mean rate of discharge of depolarizing unitary potentials as a function of the concentration of messenger according to a conventional dose–effect relationship. A separate membrane conductance, scaled by the product of an independent voltage-sensitive reaction, was included in the ICC_{MY} compartments; this was used to describe the primary component of pacemaker potentials and simulated a delay before the activation of this membrane current. The model generates pacemaker potentials and slow waves with propagation velocities similar to those determined in the physiological experiments described in the accompanying paper.

(Received 25 October 2005; accepted after revision 14 December 2005; first published online 15 December 2005)
Corresponding author F. R. Edwards: Division of Neuroscience, John Curtin School of Medical Research, Canberra, ACT, 0200, Australia. Email: frank.edwards@anu.edu.au

The preceding paper characterized the anal and circumferential spread of slow waves in the guinea-pig gastric antrum. Briefly, antral slow waves originate near the corpus and propagate slowly in an anal direction but more rapidly in a circumferential direction (Hirst *et al.* 2006). Antral slow waves are generated by two sets of interstitial cells of Cajal (ICC). Myenteric ICC (ICC_{MY}) generate pacemaker potentials (Dickens *et al.* 1999), which propagate slowly through the myenteric network of interstitial cells (Hennig *et al.* 2004; Hirst *et al.* 2006), passively depolarizing the longitudinal and circular muscle layers (Cousins *et al.* 2003). In the circular layer, each wave of pacemaker depolarization activates intramuscular ICC (ICC_{IM}): ICC_{IM} generate the secondary component of the gastric slow wave (Dickens *et al.* 2001), which then propagates rapidly in a circumferential direction (Hirst *et al.* 2006).

This paper explores what electrical parameters might give rise to the slow anal and more rapid circumferential conduction velocities of slow waves in the antrum. The approach taken was to incorporate the electrical models, which have been derived to explain the generation of slow waves in the circular layer of the guinea-pig antrum (Edwards & Hirst, 2003) and pacemaker potentials in ICC_{MY} (Edwards & Hirst, 2005), into the multidimensional cable structures making up the ICC_{MY} network and the longitudinal and circular muscle layers which form the wall of the antrum.

Methods

All the experimental data used to analyse the spread of pacemaker potentials through the myenteric network of interstitial cells and the spread of slow waves in anal and circumferential directions in the guinea-pig antrum are published in the previous paper (Hirst *et al.* 2006). All procedures used for the acquisition of physiological data from isolated tissues were approved by the Animal Experimentation Ethics Committee at the Australian National University. Guinea-pigs of either sex were stunned, exsanguinated and the stomach removed.

 DOI: 10.1113/jphysiol.2005.100743

Electrical simulations

Equivalent electrical circuit. The muscular wall of the antrum consists of two layers of smooth muscle, the longitudinal and circular layers, which are both electrically connected to the intervening layer of ICC_{MY}. The nature of the electrical connections between the three layers has been determined experimentally in a previous study (Cousins *et al.* 2003).

Longitudinal muscle layer

In this study a segment of longitudinal muscle 2 mm long and 600 μm wide was represented as the series connexion of 20 isopotential compartments, each 100 μm long (see Methods in Cousins *et al.* 2003). Small isopotential sheets of longitudinal muscle with attached networks of ICC_{MY} have been simulated previously (Edwards & Hirst, 2005). The equivalent electrical circuit for a single short, isopotential segment of longitudinal muscle (Fig. 1*A*; rightmost compartment) has previously been determined (Cousins *et al.* 2003) and the values for the background membrane conductance (g_{LM}, 110 nS) and the membrane capacitance (C_{LM}, 20 nF) of the longitudinal muscle segment used in this simulation are rounded versions of those shown in Fig. 1 of Edwards & Hirst (2005).

ICC_{MY} network

A compartment representing an isopotential sheet of ICC_{MY} network was connected to each longitudinal muscle compartment (Fig. 1*A*, central compartment) by a conductance with the value 300 nS (Cousins *et al.* 2003). Pacemaker potentials were simulated largely as previously described (Edwards & Hirst, 2005). Values for the background membrane conductance (g_{MY}, 80 nS) and the membrane capacitance (C_{MY}, 4 nF) of the ICC_{MY} compartment were again rounded versions of those used before (Edwards & Hirst, 2005). Initial calculations showed that the electrical description of the primary component of the pacemaker potential generated by ICC_{MY} (Edwards & Hirst, 2005) was unable to provide an adequate description on which to base the propagation of pacemaker potentials through the ICC_{MY} network. Except in the case of Fig. 3, the model for the primary component, $g_{Prim}(t)$ (Fig. 1*A*), was altered, with the principal change being to introduce a voltage-dependent delay between conducted depolarization and initiation of the primary component. This follows the observation on murine intestinal ICC_{MY} that the onset of the autonomous inward current, which corresponds to the primary component in guinea-pig gastric antrum in terms of duration and sensitivity to extracellular calcium ion concentration, is invariably preceded by a small but finite delay after the onset of depolarization (Goto *et al.* 2004). A single step chemical reaction was proposed to convert a precursor reagent into a messenger product as shown in eqn (1), and $g_{Prim}(t)$ was proposed to vary directly with the concentration of the product.

$$[\text{reagent}] \underset{K_{PB}}{\overset{ANK_{PF}}{\rightleftharpoons}} [\text{product}] \tag{1}$$

The forward reaction rate displayed Hodgkin-Huxley voltage sensitivity (Hodgkin & Huxley, 1952). The maximum forward rate of production of product, K_{PF}[reagent], was made 0.012 s^{-1} and the reverse rate constant, K_{PB}, was made 6 s^{-1}. The steady state activation, A_∞, and the steady state inactivation, N_∞, varied with membrane potential as shown in Fig. 1*C*. The time constant for activation, τ_A, had the value 60 ms at all values of membrane potential as shown in Fig. 1*C*. That for inactivation, τ_N, was voltage dependent and is also shown in Fig. 1*C*. The following eqns (2) were used to calculate A and N, which together with K_{PF} and K_{PB} yielded the time course of [product].

$$\begin{aligned}
A_\infty &= 1/\left(1 + e^{0.78(-48-E_m)}\right)\\
\frac{dA}{dt} &= \frac{A_\infty - A}{\tau_A}\\
\tau_A &= 0.06\ \text{s}\\
N_\infty &= 1/\left(1 + e^{(E_m+53)}\right)\\
\frac{dN}{dt} &= \frac{N_\infty - N}{\tau_N}\\
\tau_N &= 0.25 + 89.75/\left(1 + e^{2(E_m+48)}\right)\ \text{s}
\end{aligned} \tag{2}$$

The value of $g_{Prim}(t)$ was made to vary directly with [product] as stated in eqn (3):

$$g_{Prim}(t) = G_{Prim}[\text{product}] \tag{3}$$

where $G_{Prim} = 2.442 \times 10^7\ \mu\text{S mM}^{-1}$.

The model for the messenger-dependent unitary conductance, $g_{Plat}(t)$, was implemented with the parameters previously described (Edwards & Hirst, 2005) except that the maximum rate of production of the intermediate reagent, K_F[precursor], was reduced from 0.168 mM s^{-1} to 0.086 mM s^{-1} and τ_m was reduced from 0.25 s to 0.15 s. These refinements improved the accuracy of the wave propagation simulations without reducing the performance of the isopotential equivalent short segment model used previously (Edwards & Hirst, 2005). The value used for the conductance connecting adjacent compartments of ICC_{MY} (g_{ICC}, Fig. 1*B*) was 2800 μS. Since there is no appearance of directional asymmetry in the antral ICC_{MY} network (Hennig *et al.* 2004) and the conduction velocity of pacemaker potentials in the circumferential and anal direction did not differ significantly (Hirst *et al.* 2006), the ICC_{MY} compartments were assumed to be equally well connected in the

oro-anal direction and in the circumferential direction as shown in Fig. 1*B* (g_{ICC}). The conductance connecting one longitudinal muscle compartment axially to the next in the oro-anal direction (Fig. 1*B*, g_{LLA}) was set to 5764 μS. Cousins *et al.* (1993) obtained a mean value of 631 μm for the axial length constant of longitudinal muscle layer in guinea-pig ileum. The values chosen for connexion of ICC_{MY} compartments and longitudinal muscle compartments in the oro-anal direction allowed simulation of this estimate of passive electrical length constant and also of the propagation velocity of pacemaker and follower potentials in the anal direction. The transverse length constant for guinea-pig ileal longitudinal muscle was 59 μm (Cousins *et al.* 1993). As length constant varies inversely with the square root of the internal resistance of the equivalent cable (Jack *et al.* 1983), the transverse connecting conductance (Fig. 1*B*, g_{LLT}) was made 50.4 μS.

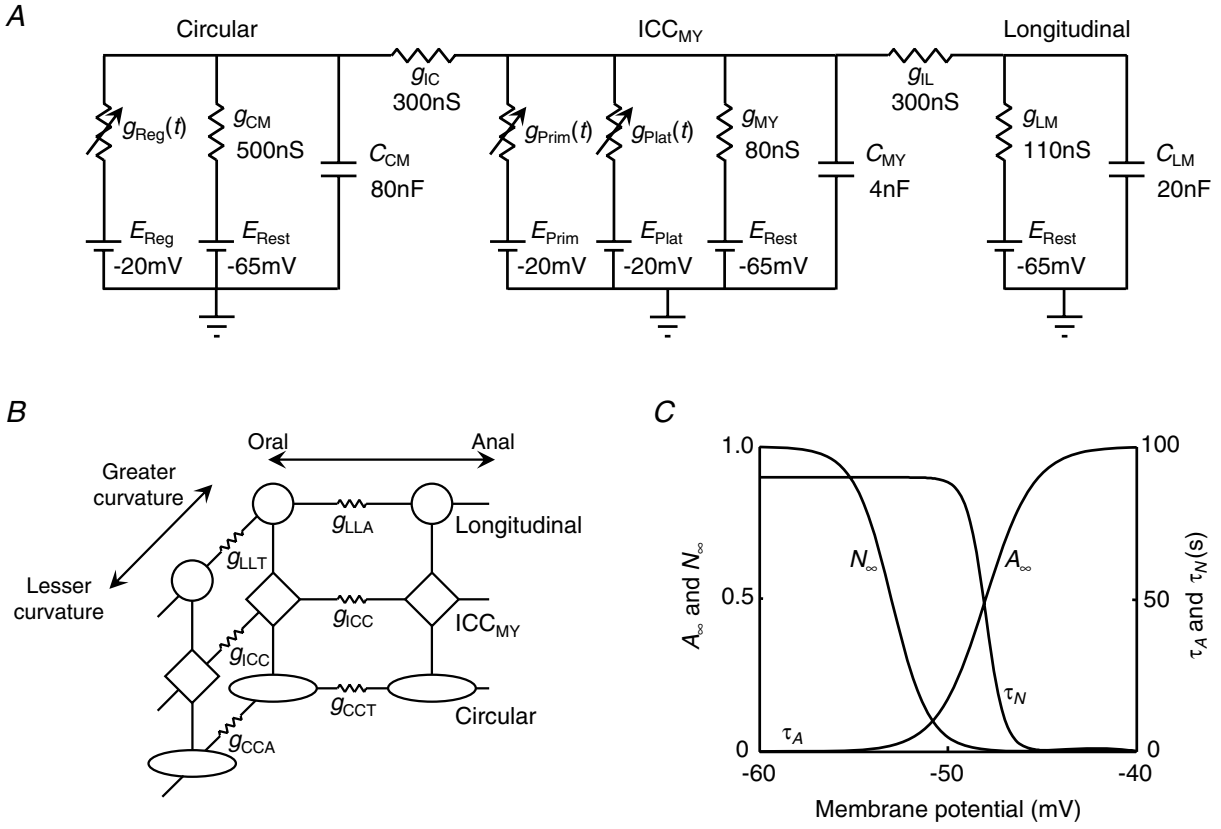

Figure 1. Equivalent electrical circuits and $g_{Prim}(t)$ gating and kinetics
A represents an intact patch of antral tissue. An isopotential segment of circular layer is represented by a linear background conductance, g_{CM}, with equilibrium potential equal to the rest potential, E_{Rest}; $g_{Reg}(t)$ represents the regenerative conductance due to unitary discharge in ICC_{IM} with equilibrium potential, E_{Reg}. C_{CM} represents the total membrane capacitance of the circular muscle layer. Similarly g_{MY} represents the background conductance of the attached ICC_{MY} network with equilibrium potential equal to the rest potential for ICC_{MY}, E_{Rest}; $g_{Prim}(t)$ represents the voltage-sensitive primary conductance and $g_{Plat}(t)$ the plateau conductance due to unitary discharge in ICC_{MY} with equilibrium potentials E_{Prim} and E_{Plat}, respectively. C_{MY} represents the total membrane capacitance of the ICC_{MY} network. The associated longitudinal muscle compartment consists of a background conductance, g_{LM}, with equilibrium potential equal to the rest potential, E_{Rest}, in parallel with C_{LM} representing the membrane capacitance of the longitudinal muscle. The electrical connexions of the ICC_{MY} network to the circular layer and to the longitudinal layer are represented by g_{IC} and g_{IL}, respectively. Component values shown are rounded versions of those derived in Edwards & Hirst (2005). *B* shows three complete antral segments (as shown in *A*); longitudinal muscle layers represented by circles, patches of ICC_{MY} network represented by diamonds and circular muscle layers represented by ellipses. Two segments are connected in the oro-anal orientation; longitudinal muscle layers connected via conductance g_{LLA}, ICC_{MY} networks connected via conductance g_{ICC} and circular muscle layers connected via conductance g_{CCT}. Likewise two segments are connected in the circumferential orientation; longitudinal muscle layers connected via conductance g_{LLT}, ICC_{MY} networks again connected via conductance g_{ICC} and circular muscle layers connected via conductance g_{CCA}. *C* shows functions for the gating variables of the forward rate of reaction leading to product sensitive changes in $g_{Prim}(t)$ (see eqn (1), (2) and (3)); the voltage dependence of steady state activation, A_∞, and steady state inactivation, N_∞, and associated time constants, τ_A, which takes the value 0.06 s for all values of membrane potential and so appears coincident with the time axis, and τ_N.

Circular muscle equivalent cable

Conduction of slow waves in the circumferential direction proceeded at 13.9 mm s^{-1} in intact tissue (Hirst *et al.* 2006). Experiments on preparations of antrum where the longitudinal muscle layer and accompanying ICC_{MY} network had been removed, except for a band near the greater curvature, showed that normal slow waves persisted throughout the circular muscle layer. Circumferential conduction velocity in the region devoid of ICC_{MY} was 14.7 mm s^{-1} which was not significantly different from that in intact tissue (Hirst *et al.* 2006). Therefore, to model circumferential electrical propagation in the antrum, a segment of a circular muscle bundle 9.6 mm long was represented as the series connexion of 16 isopotential compartments, each 600 μm long and 100 μm wide (see Methods in Cousins *et al.* 2003). The passive length constant of a bundle of antral circular muscle is about 3 mm (Hirst *et al.* 2006) so a chain of 16 compartments represented about three length electrical constants. The equivalent electrical circuit for a single short, isopotential segment of circular muscle bundle (Fig. 1*A*; leftmost compartment) has previously been determined (Edwards & Hirst, 2003) and the values for the background membrane conductance (g_{CM}, 500 nS) and membrane capacitance (C_{CM}, 80 nF) used in this simulation are rounded versions of those used previously (Edwards & Hirst, 2005). The model for messenger-dependent unitary conductance, $g_{Reg}(t)$, was implemented with the parameters previously described (Edwards & Hirst, 2005) except that the maximum rate of production of the intermediate reagent, K_F[precursor], was doubled from 0.0196 mM s^{-1} to 0.0392 mM s^{-1}. While this modification increased the peak amplitude of the simulated slow wave to a value near the upper end of the observed range, it also increased the onset rate to a value close to that seen in physiological experiments. Onset rate had not been a critical measure in the case of a single compartment; however, simulations indicated that conduction velocity varied with the initial rate of depolarization which determined the time taken for a neighbouring compartment to reach regenerative threshold. Therefore a better match of this characteristic was important in this multi-compartment model. This increase in K_F[precursor] permitted successful simulation of slow wave propagation velocity (see Fig. 4); the onset latency of the regenerative component of the slow wave was well simulated following this adjustment. The conductance connecting one isopotential compartment axially with the adjacent compartment in the same circular muscle bundle (Fig. 1*B*, g_{CCA}) was set to 11.9 μS to model the passive electrical length constant in the axial direction along the bundle (3 mm; Hirst *et al.* 2006). As circular muscle bundles were found to be poorly connected to adjacent bundles with failures of conduction every few bundles (Hirst *et al.* 2006), the value of g_{CCT} (Fig. 1*B*) was set to zero.

Corporal circular muscle pacing

When modelling conduction of slow waves in the circumferential direction, pacing of the ICC_{MY} network was provided by a corporal circular muscle equivalent compartment (Fig. 6). The model used to describe the corpus was similar to that for a segment of antral circular muscle bundle (Edwards & Hirst, 2005) with the value for τ_h, the rate of recovery from inactivation at hyperpolarized membrane potentials, reduced from 6 s to 3.8 s to allow generation of slow waves at the higher rate of discharge seen in the corpus (Hashitani *et al.* 2005). This modification allowed simulation of corporal slow waves which reflected the range of amplitudes and peak negative membrane potentials encountered in the corpus (Hashitani *et al.* 2005).

Passive length constants

Plots of passive length constants (Figs 3*A*, 4*A*, 5*A* and 6*A*) were determined by injecting a current into the most oral longitudinal muscle compartment (or circular muscle compartment in Fig. 6) after voltage-dependent mechanisms had been disabled, and measuring the voltage response in each other muscle compartment. The apparent length constant at a compartment was then calculated using the distance from the most oral compartment and the ratio between the steady state voltage response in the most oral compartment and the steady state voltage response in the compartment under test. Since the cables modelled were of finite length, the length constant calculated in this way increased as the anal end of the cable was approached due to reflection of current (Jack *et al.* 1983). Measurements of conduction velocity were made in regions of the cable models which were sufficiently proximal that the measured length constant was within 10% of its design value. The passive length constant plots have been included to underline that the speed measurements were carried out over regions of approximately uniform apparent length constant.

Simulations were carried out using MatLab 7.0.4.365 (R14) SP2 (The MathWorks, Natick, MA, USA). Stiff differential equation solver ode15s was used. Computations were carried out on an Intel Pentium 4-based desktop computer.

Results

Initiation of pacemaker potentials in a network of ICC_{MY}

The approach taken in this study has been to link together 20 pacemaker compartments whose properties

matched those determined experimentally when recording pacemaker potentials from ICC_{MY} located in isolated short segments of antral wall (Cousins *et al.* 2003). To examine the constraints imposed on the conduction of pacemaker potentials through a network of ICC_{MY} when several ICC_{MY} and attached longitudinal muscle compartments were connected together, the first aspect considered was what conditions were required for pacemaker potentials to be initiated such that they swept in an anal direction with a conduction velocity of 3.5 mm s^{-1} (Hirst *et al.* 2006). The objective was to achieve a propagation velocity near the average value recorded in physiological experiments while adhering as closely as possible to the parameter values arrived at in previous models of individual isopotential compartments (Edwards & Hirst, 2003, 2005). In initial simulations, all ICC_{MY} compartments were given the same membrane conductance parameters and initial conditions; similarly, all longitudinal muscle compartments were made identical. Thus, all cells discharged in tandem with theoretically zero phase difference in each case. In fact, the stochastic nature of the generation of unitary potentials in the ICC_{MY} compartments resulted in small phase differences; however, these differences varied from wave to wave (Fig. 2*A*). Thus, on some occasions, a pacemaker potential would first arise in an orally located compartment and propagate in an anal direction (Fig. 2*Bc*). On other occasions, an anally located compartment would discharge the first

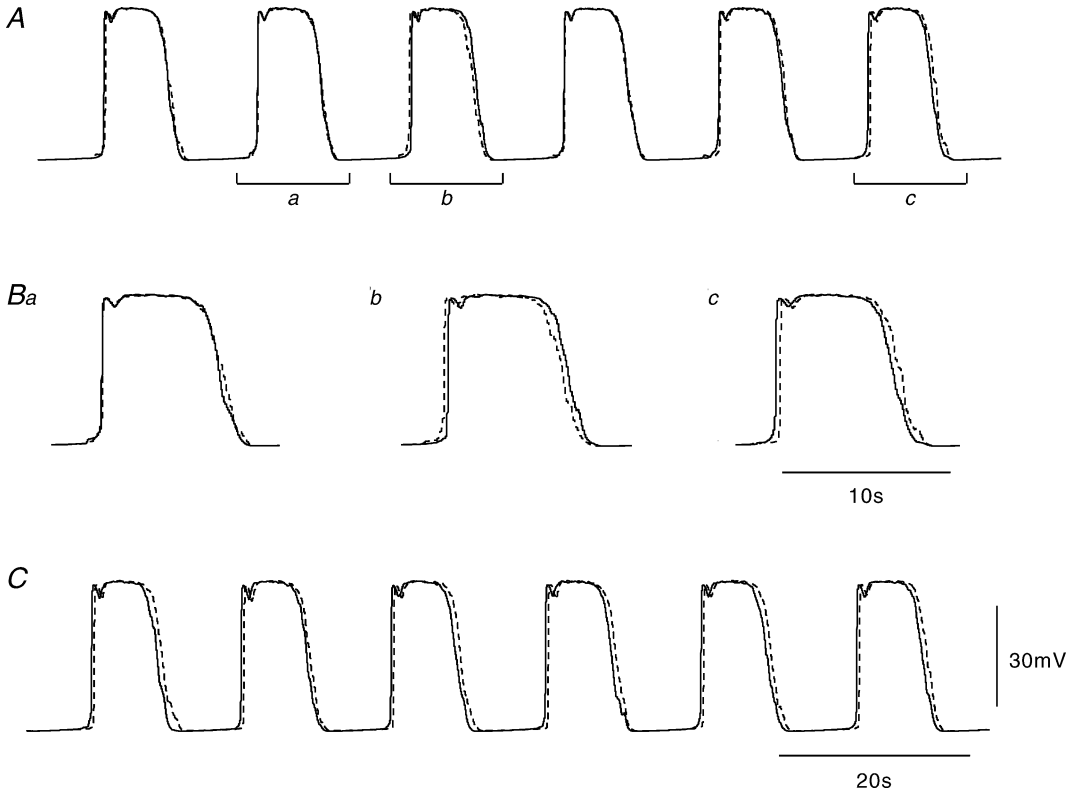

Figure 2. Direction of pacemaker potential propagation
A shows simulations of pacemaker potentials generated by ICC_{MY} compartments numbers 2 (continuous line) and 12 (dashed line; 1 mm separation) in a chain of 20 compartments. Each ICC_{MY} compartment was attached to a longitudinal muscle compartment. All ICC_{MY} compartments shared identical passive and active conductance parameters and identical initial conditions. Likewise, all longitudinal muscle compartments shared identical parameters and identical initial conditions. Thus, any differences between voltages in ICC_{MY} compartments were due to statistical differences in the discharges of unitary conductances in each of the ICC_{MY} compartments. In this figure only, the cable was made electrically short; the conduction velocity was therefore slow, allowing clear demonstration of conduction delays. Note that there is not a consistent direction of conduction. *B* shows expansions of three pairs of pacemaker potentials shown in *A*. *Ba* shows pacemaker potentials occurring almost simultaneously in both compartments (bar a in *A*). *Bb* shows pacemaker potentials starting near compartment 12 and propagating to compartment 2 (bar *b* in *A*). *Bc* shows pacemaker potentials starting near compartment 2 and propagating to compartment 12 (bar *c* in *A*). *C* shows the results of the same calculation when, for the primary component of the first compartment, the activation and inactivation curves were displaced leftwards by 1 mV (Fig. 1*C*). Note that the rate of discharge is similar, but now the direction of propagation is consistently from compartment 2 toward compartment 12. The time scale bar on *C* applies to *A* also. The amplitude scale bar refers to all traces.

pacemaker potential and this would propagate in an oral direction (Fig. 2*Bb*). Simultaneous occurrence of pacemaker potentials in well separated compartments was also seen (Fig. 2*Ba*). Therefore a constant direction of wave propagation was not maintained under these conditions. The physiological correlate of this behaviour has been observed in isolated preparations of antrum (Ward *et al.* 2004; Hirst *et al.* 2006). To impart a direction to propagation of pacemaker potentials along the strip of longitudinal muscle and associated ICC_{MY} network, the primary conductance (Fig. 1*A*, $g_{Prim}(t)$) in the ICC_{MY} compartment at one end of the chain was allotted a voltage threshold marginally more negative (1 mV) than was the case in the other ICC_{MY} compartments. Therefore this first compartment, in isolation, had a rate of discharge slightly faster than that of the other compartments and introduced only a minor inhomogeneity, meant to represent pacemaking input from the corpus, into one end of the equivalent cable. This resulted in pacemaker potentials that propagated consistently in a single direction (Fig. 2*C*). The model used to generate the data shown in Fig. 2 was adjusted to discharge spontaneous pacemaker potentials at close to 4 waves min^{-1}, so that a small change in threshold produced a constant direction of propagation with little increase in overall discharge rate. Furthermore, the cable model used to generate Fig. 2 was made electrically shorter than those encountered in physiological experiments. This resulted in a slowed conduction velocity in order to emphasize propagation delays.

The model for generation of electrical activity by ICC_{MY} (Edwards & Hirst, 2005), which included an estimate of the values of coupling conductance between each ICC_{MY} compartment and its adjacent muscle compartments (Fig. 1*A*, g_{IC}), was extended to examine the conduction of pacemaker potentials along the oro-anal axis. The coupling conductances between successive ICC_{MY} compartments and those between adjacent compartments of longitudinal muscle were varied widely in an attempt to match both the estimated passive length constant of the longitudinal layer (631 μm, Cousins *et al.* 1993) and the measured propagation velocity of pacemaker potentials (3.5 mm s^{-1}, Hirst *et al.* 2006). A satisfactory solution could not be achieved. For example, if low resistance pathways existed between adjacent ICC_{MY}, or if the longitudinal muscle layer was well connected, rapid conduction occurred. Thus, when the conduction velocity was correctly matched, the associated length constant was too short. Conversely, if the passive length constant was matched the conduction velocity was too rapid. Figure 3 shows one such case in which the conductance connecting ICC_{MY} compartments (Fig. 1*B*, g_{ICC}) was set to 0 μS and that connecting longitudinal muscle compartments in an oro-anal direction (Fig. 1*B*, g_{LLA}) was set to 6600 μS (see Methods). This combination of coupling conductances yielded the slowest propagation speed for the desired length constant. The discharge rate and direction of pacemaker potential propagation were maintained by allotting the most oral ICC_{MY} compartment activation and inactivation curves for $g_{Prim}(t)$ displaced by −10 mV compared with those describing $g_{Prim}(t)$ in each other compartment. This faster oscillation of the first ICC_{MY} compartment was used to initiate pacing in all further simulations. It can be seen that the passive length constant is close to 631 μm (Fig. 3*A*, dotted line) for most of the cable including that segment between the points of measurement. However, the conduction velocity between the second and twelfth compartments was 4.4 mm s^{-1}, which was some 30% faster than the measured value of 3.5 mm s^{-1} (Hirst *et al.* 2006).

Clearly the preceding approach could not provide an adequate description of physiological data with the simple

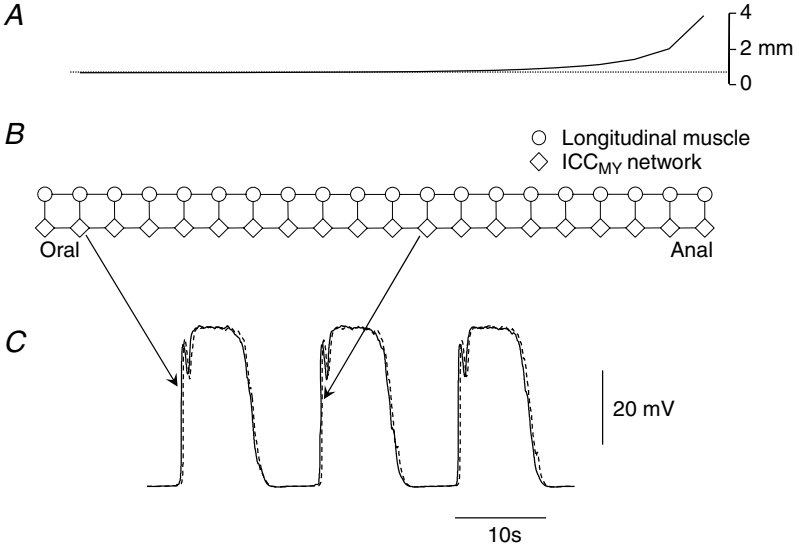

Figure 3. Pacemaker potential propagation in the anal direction when the primary component is modelled as a voltage-sensitive membrane conductance
A shows the passive length constant (see Methods) for a chain of 20 ICC_{MY} compartments and 20 attached longitudinal muscle compartments shown schematically in *B*. The dotted line in *A* shows the mean axial length constant for longitudinal muscle of 631 μm estimated from physiological data (Cousins *et al.* 1993). *C* shows simulations of pacemaker potentials generated by ICC_{MY} in compartment 2 (solid line) and compartment 12 (dashed line). The primary component in each ICC_{MY} compartment was modelled as previously described by Edwards & Hirst (2005). The elapsed time between pacemaker potentials occurring in these compartments 1 mm apart was 225 ms. This corresponded to a propagation speed of 4.4 mm s^{-1}.

description of pacemaker activity used previously. The simulation of ICC_{MY} electrical activity shown in Fig. 3 used a model for the primary component (Fig. 1*A*, $g_{Prim}(t)$) which responded rapidly to conducted depolarization (Edwards & Hirst, 2005). However, Goto *et al.* (2004) describe an autonomous inward current in isolated mouse intestinal ICC_{MY}. When this current was activated it displayed an autonomous time course, lasting about 500 ms regardless of the duration of the initiating depolarization. Furthermore, the autonomous inward current displayed a brief, membrane potential-dependent delay of 20–200 ms following applied depolarization. The conduction velocity of pacemaker potentials is determined by the onset latency of the primary component once local voltage threshold is reached. Therefore, since the properties of the initial component of antral and intestinal ICC_{MY} are very similar (Hirst & Edwards, 2001; Kito *et al.* 2002, 2005; Kito & Suzuki, 2003), the model previously used for the primary component of antral pacemaker potentials was altered to include a brief voltage-dependent delay between the arrival of conducted depolarization and the onset of the primary component (see Methods). The coupling conductance between adjacent ICC_{MY} compartments was made 2800 μS and that between adjacent compartments of longitudinal muscle was made 5764 μS so as to match the estimated passive length constant (631 μm; Cousins *et al.* 1993). These selections yielded similar length constants for an isolated ICC_{MY} equivalent cable (590 μm) and an isolated longitudinal muscle equivalent cable (720 μm) – values that are not accessible to experimental verification due to the limitations of dissection. The result of the computation is shown in Fig. 4. As in Fig. 3*A*, the passive length constant for the cross-connected cable pair is close to the design value of 631 μm (Fig. 4*A*, dotted line). However, using the altered model for $g_{Prim}(t)$, the propagation velocity between the second and twelfth compartments was 3.3 mm s^{-1} which was close to the average speed seen in the physiologically acquired records (3.5 mm s^{-1}, Hirst *et al.* 2006).

Slow waves travel around the circumference of the antrum more quickly (14.7 mm s^{-1}) than pacemaker potentials travel down the greater curvature (3.5 mm s^{-1}, Hirst *et al.* 2006). However, the propagation speed of pacemaker potentials in the ICC_{MY} network is similar in both circumferential and anal directions after removal of circular muscle sheet (3.5 mm s^{-1}, Hirst *et al.* 2006). It seemed possible that the simple addition of a passive circular muscle current pathway in the circumferential orientation might alone be sufficient to account for the observed difference in propagation speed. Therefore it was of interest to see at what speed pacemaker potentials would propagate around the circumference of the stomach if sustaining the wave were due to the action of ICC_{MY} in the absence of ICC_{IM}. The model used to generate the data shown in Fig. 4 was

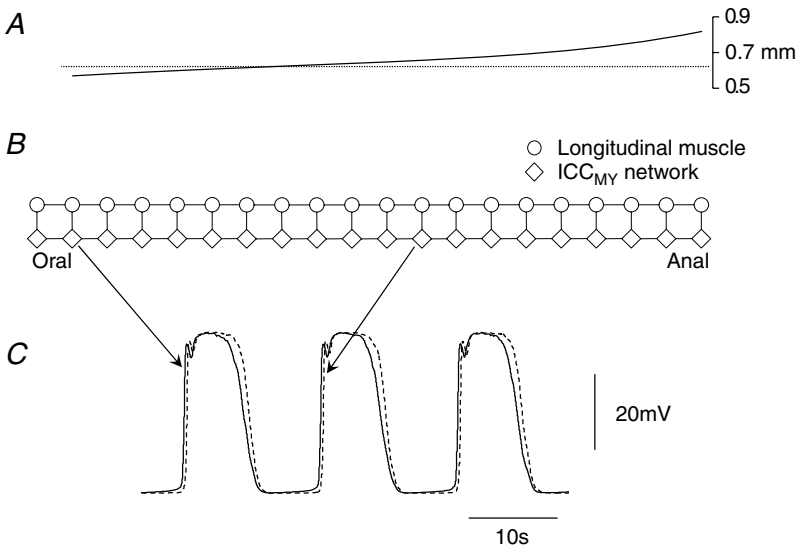

Figure 4. Pacemaker potential propagation in the anal direction when the primary component is modelled as a voltage-sensitive chemical reaction and product-sensitive membrane conductance
A shows the passive length constant (see Methods) for a chain of 20 ICC_{MY} compartments and 20 attached longitudinal muscle compartments shown schematically in *B*. The dotted line in *A* shows the mean axial length constant for longitudinal muscle of 631 μm estimated from physiological data (Cousins *et al.* 1993). *C* shows simulations of pacemaker potentials generated by ICC_{MY} in compartment 2 (continuous line) and compartment 12 (dashed line). The primary component in each ICC_{MY} compartment was modelled as a conductance proportional to the concentration of a reaction product with the rate of production being sensitive to membrane potential (see Methods). The elapsed time between pacemaker potentials occurring in these compartments 1 mm apart was 300 ms. This corresponded to a propagation speed of 3.3 mm s^{-1}.

altered in two ways. Firstly, the conductances connecting longitudinal muscle compartments were set to 50.4 μS to correspond to g_{LLT} (Fig. 1*B*). This was necessary because the direction of follower potential conduction is in this case transverse to the axis of the longitudinal muscle cells. Since the ICC_{MY} network is assumed to be isotropic, the conductance connecting ICC_{MY} compartments remained unchanged (Fig. 1*B*, g_{ICC}). The propagation speed of pacemaker potentials was measured in this circumferentially orientated network before circular muscle compartments were added, to check that it was similar to that in the anal direction, as seen in the physiological records (Hirst *et al.* 2006). Pacemaker potentials propagated at 2.7 mm s^{-1} or about 18% slower than in the anal direction. The mean values for propagation velocities of follower potentials along and across the longitudinal muscle layer after removal of the circular layer were 3.7 mm s^{-1} and 3.2 mm s^{-1}, a difference of 14% and in the same direction as the simulation (Hirst *et al.* 2006). The second alteration to the model was the connection of a circular muscle compartment to each ICC_{MY} compartment, as is the case for intact antral tissue. The circular muscle compartments were each connected to the adjacent circular muscle compartment (Fig. 5*B*) via conductances of value 11.9 μS to give a passive length constant of 3 mm (see Methods) (Hirst *et al.* 2006). Furthermore, the circular muscle compartments were made passive by omitting $g_{Reg}(t)$ (Fig. 1*A*) from each compartment. These modifications changed the measured length constant of the ICC_{MY} network and attached longitudinal and circular muscle layers to about 200 μm (Fig. 5*A*; continuous line). The propagation velocity between the second and twelfth compartments was found to fall to 1.6 mm s^{-1}, much slower than the velocity, 14.7 mm s^{-1}, measured from the physiological data (Hirst *et al.* 2006). Thus, adding the circular muscle pathway actually slowed the propagation speed from 2.7 mm s^{-1} to 1.6 mm s^{-1} rather than speeding it. This was because the circular muscle membrane provided additional pathways for the propagating current to flow to the extracellular environment as well as to adjacent ICC_{MY} compartments. This speed reduction mirrored that found in the comparison between slow waves in intact antrum (2.5 mm s^{-1}) and those after removal of the circular layer (3.5 mm s^{-1}, Hirst *et al.* 2006). Therefore circumferential conduction of current via an added passive circular muscle pathway is unlikely to account for the rapid circumferential propagation of slow waves; it in fact would be expected to slow the radial conduction velocity.

Finally, how the activity of ICC_{IM} contained within the circular muscle bundle altered slow wave conduction in the circumferential direction was explored. Figure 6 illustrates a chain of 16 circular muscle compartments, each including a proportion of ICC_{IM} which contribute

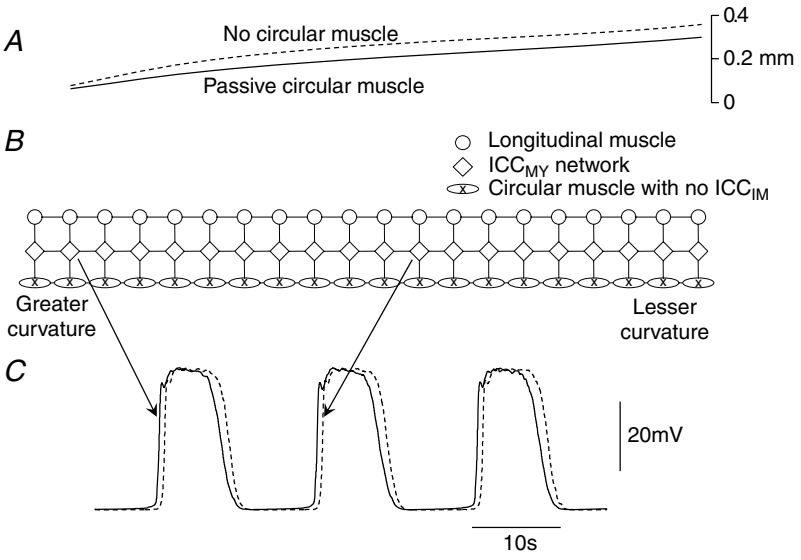

Figure 5. Circumferential propagation of pacemaker potentials in an ICC_{MY} network with attached transverse longitudinal muscle and passive circular muscle bundle
A shows the passive length constant (see Methods) for a chain of 20 ICC_{MY} compartments and 20 attached longitudinal muscle compartments (dashed line). Note that in this case the longitudinal muscle compartments were connected transversely rather than axially, as was the case in Figs 3 and 4, so the length constant is shorter owing to the reduced access between longitudinal muscle compartments. The continuous line shows the passive length constant after a chain of circular muscle compartments (ellipses labelled x) was attached to the ICC_{MY} chain as shown schematically in *B*. *C* shows simulations of pacemaker potentials generated by ICC_{MY} in compartment 2 (continuous line) and compartment 12 (dashed line). The elapsed time between pacemaker potentials occurring in these compartments 1 mm apart was 615 ms. This corresponded to a propagation speed of 1.6 mm s^{-1}.

depolarizing current via $g_{Reg}(t)$ (Fig. 1*A*). These compartments were connected axially and so reached around the stomach in a circumferential orientation. The conductance connecting circular muscle compartments (Fig. 1*B*, g_{CCA}) was set to 11.9 μS which resulted in a length constant of close to 3 mm (Hirst *et al.* 2006) for most of the equivalent cable (Fig. 6*A*). The six compartments closest to the greater curvature were each connected to an ICC_{MY} compartment which was in turn connected to a longitudinal muscle compartment. Each ICC_{MY} compartment was connected to the adjacent ICC_{MY} compartments (g_{ICC}, Fig. 1*B*). Each longitudinal muscle compartment was connected to the adjacent longitudinal muscle compartments (g_{LLT}, Fig. 1*B*). Pacing was provided by a corporal circular muscle compartment attached to the ICC_{MY} compartment nearest the greater curvature (Fig. 6*B*; see Methods). Therefore, a driving potential was initiated in this ICC_{MY} compartment, propagated to and was supported by the adjacent ICC_{MY} and was conducted to the circular muscle compartments connected to the ICC_{MY} compartments to provide the initial component of the slow wave. The circular muscle compartments sequentially provided regenerative components to complete the slow wave, which was conducted in the direction of the lesser curvature. The slow wave was conducted into circular muscle compartments which had no direct connexion with ICC_{MY}, but was nonetheless maintained in amplitude and conduction velocity. In the circular muscle compartments further from the greater curvature, the initial component of the slow wave was reduced or absent (Fig. 6*C*, dashed line). The slow wave conduction velocity sustained in this cable model was 14 mm s^{-1}, which was close to that recorded in circular muscle preparations with only a small band of ICC_{MY} network left near the greater curvature to initiate each slow wave (14.7 mm s^{-1}, Hirst *et al.* 2006).

Discussion

This report has examined the electrical requirements necessary to allow the antrum to generate the characteristic patterns of electrical activity detected experimentally. They offer an explanation of how slow waves spread rapidly around the stomach in a circumferential direction, making a ring of contraction, which progresses more slowly down the stomach in an anal direction. Given the electrical complexity of the stomach wall it has been necessary to design an electrical model in which three distinct sets of electrical cables are linked together. One cable was made of chains of longitudinal muscle compartments, a second was made up of a chain of ICC_{MY} with the third being a chain containing a mixture of circular smooth muscle cells and ICC_{IM}, orientated at right angles to the longitudinal muscle chain. The values of the communicating conductances

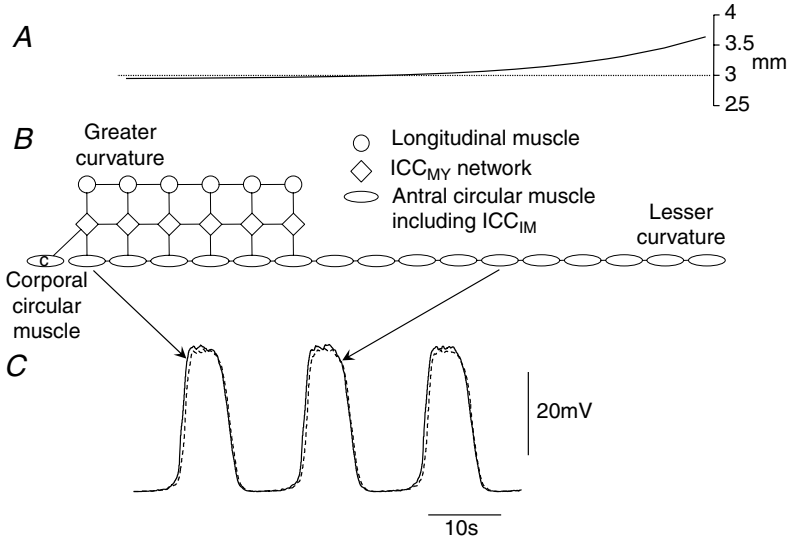

Figure 6. Circumferential propagation of slow waves in a bundle of circular muscle
A shows the passive length constant (see Methods) for a chain of 16 circular muscle compartments shown schematically in *B*. The dotted line in *A* shows the mean axial length constant for circular muscle of 3 mm obtained from physiological data (Hirst *et al*. 2006). Also shown in *B* is a chain of 6 ICC_{MY} compartments and attached longitudinal muscle compartments. The ICC_{MY} compartment nearest the greater curvature was paced by an attached corporal circular muscle compartment (ellipse labelled c). The ICC_{MY} compartments generated driving potentials which initiated slow waves in the circular muscle bundle. Slow waves propagated to regions of the circular muscle bundle which were not directly attached to ICC_{MY} compartments. *C* shows simulations of slow waves generated in circular muscle compartment 2 (continuous line) and compartment 12 (dashed line). The elapsed time between slow waves occurring in these compartments 6 mm apart was 430 ms. This corresponded to a propagation speed of 14 mm s^{-1}.

between the three compartments have been determined experimentally (Cousins *et al.* 2003) and the ICC_{MY} and circular muscle cables generated active responses using analytical solutions defined previously (Edwards & Hirst, 2003, 2005).

When the model was set up using a chain of ICC_{MY} with identical properties, pacemaker potentials originated at different points along the chain (Fig. 2). This behaviour is detected in physiological recordings from isolated regions of the antrum (Hennig *et al.* 2004; Ward *et al.* 2004; Hirst *et al.* 2006) but does not occur in the intact stomach (Szurszewski, 1981; Davenport, 1989). An anally directed progression of pacemaker potentials in the ICC_{MY} network could be achieved by making more negative the activation potential of the initial component of the pacemaker potential of the most oral node in the ICC_{MY} network. The alternative approach was to provide a stimulus at the oral end of the chain of ICC_{MY} with a higher frequency of occurrence than that naturally generated by the ICC_{MY} network. In the intact stomach such a stimulus is provided by the corpus which generates slow waves with a higher frequency of discharge than that of the isolated antrum (Hashitani *et al.* 2005). When attached to the corpus, the natural frequency is entrained to be the same as that of the corpus (Hashitani *et al.* 2005). A pacemaker potential initiated in the most orally located compartment proceeded strictly in an anal direction as the refractory characteristics of the primary and regenerative components prevented backfiring along the cable.

Pacemaker potentials propagate very slowly in an anal direction. Furthermore, after removal of the circular layer, their conduction velocities in the anal and circumferential directions are similar (Hirst *et al.* 2006). In such preparations, the ICC_{MY} network is connected solely to the longitudinal muscle layer by a finite, predetermined resistance (Cousins *et al.* 2003). Previous studies on the longitudinal muscle layer have indicated that its passive electrical length constants are asymmetrical, more readily allowing current flow in an oro-anal direction (Cousins *et al.* 1993; see also Hirst *et al.* 2006), so giving rise to different conduction velocities of action potentials in the two directions (Stevens *et al.* 1999). The simplest explanation for the slow propagation of pacemaker potentials in the anal direction might be that the resistance between adjacent ICC_{MY} was very high. This seems an unlikely explanation since dyes readily move though the ICC_{MY} network (Dickens *et al.* 1999) and numerous gap junctions are found in the network (Jimenez *et al.* 1999). When this proposition was tested using a simulation it was found possible to slow the propagation velocity markedly by making the resistance between ICC_{MY} very high. This meant that current flow for propagation occurred almost solely via the longitudinal muscle layer. However, given the asymmetry of longitudinal muscle passive length constants in the oro-anal and circumferential directions, the conduction velocity in the circumferential direction fell even more dramatically. Clearly this is not in accord with the finding that the conduction velocity of pacemaker potentials, in preparations containing only ICC_{MY} and longitudinal muscle, is very similar in the longitudinal and circumferential directions (Hirst *et al.* 2006). An alternative explanation was sought. In their description of the electrical properties of murine intestinal ICC_{MY}, Goto *et al.* (2004) found that the onset of the initial component of the pacemaker potential occurred after a brief but finite delay. Thus the electrical description of pacemaker activity was modified to incorporate this behaviour. When this was done, even though an appreciable part of the current necessary to allow propagation of pacemaker potentials continued to flow though the longitudinal layer, appropriate simulations of conduction velocity in the anal and circumferential directions could be achieved (Fig. 4).

Slow waves conduct faster in a circumferential direction than do pacemaker potentials in an anal direction. Having found that the spread of pacemaker activity could be influenced by the electrical properties of the cells to which ICC_{MY} were coupled, the effect of adding a circular muscle chain to the model was examined. It was found that since this layer had such a low input resistance, rather than increasing the circumferential conduction velocity of pacemaker potentials, the current drain actually reduced the circumferential conduction velocity (Fig. 5). As it had been found that ICC_{MY} were not required for the circumferential spread of slow waves, the effect of introducing the regenerative component of the slow wave was examined.

Circumferential spread of the slow waves takes place within the circular muscle layer, outpacing circumferential spread of pacemaker potentials via the ICC_{MY} network and associated longitudinal muscle layer. Presumably waves in ICC_{MY} which lie far from the greater curvature are initiated by slow waves in the underlying circular muscle, although no physiological experiments have been conducted to examine this point. Hence, when the longitudinal muscle and the ICC_{MY} network are removed from a sheet of circular muscle, except for a band near the greater curvature, normal slow waves persist throughout the circular muscle layer (Hirst *et al.* 2006). Likewise, anally directed progression of electrical activity appears to be carried mainly by the ICC_{MY} network and associated longitudinal muscle layer. When the circular muscle layer is removed, pacemaker potentials continue to propagate through the remaining layers in an anal direction at an unchanged speed (Hirst *et al.* 2006). Moreover the poor and variable oro-anal connectivity between circular muscle bundles will prohibit extensive oro-anal conduction in the circular layer. A model comprising 16 circular muscle compartments, each isopotential, and together representing about three length constants of cable was chosen. With minor alterations to

the parameters specified by Edwards & Hirst (2005) (see Methods) slow waves propagated along this equivalent circular muscle bundle at 14 mm s^{-1} which was close to 14.7 mm s^{-1}, the speed measured in the tissue after removal of most of the ICC_{MY} layer (Hirst *et al.* 2006). The predictive power of the model offered is limited by the accuracy of the kinetic models used for the primary and plateau components of the pacemaker potential in the ICC_{MY} network and the regenerative potential in circular muscle compartments. The simplified reactions leading to increased discharge of unitary events may not be precise. Furthermore, some voltage-dependent membrane currents exist in both circular and longitudinal smooth muscle cells which have been treated as ohmic in these simulations. However, the model as described is able to mimic a suite of behaviours seen in physiological experiments on antral tissue. Extension of the model to incorporate other regions of stomach and neural contributions may lead to a more rapid understanding of the locus and genesis of gastric dysrhythmias and other clinical conditions.

In summary, pacemaker depolarizations originating in the gastric corpus conduct slowly in an anal direction presumably via the ICC_{MY} network and associated longitudinal muscle layer, their propagation speed limited by the onset latency of the primary component of the antral pacemaker potential. Excitation of circular muscle bundles occurs at the region of largest ICC_{MY} density, the greater curvature, and spreads rapidly around the stomach via small groups of adjacent circular muscle bundles. The amplitude and speed of the circumferential slow wave and associated contraction is maintained by ICC_{IM} within the circular muscle bundles. The rapid circumferential spread of the slow wave forms a ring of contraction around the stomach which moves in an anal direction at about 3.5 mm s^{-1}, propelling the gastric contents towards the gastro-duodenal junction.

References

Cousins HM, Edwards FR, Hickey H, Hill CE & Hirst GDS (2003). Electrical coupling between the myenteric interstitial cells of Cajal and adjacent muscle layers in the guinea-pig gastric antrum. *J Physiol* **550**, 829–844.

Cousins HM, Edwards FR, Hirst GDS & Wendt IR (1993). Cholinergic neuromuscular transmission in the longitudinal muscle of the guinea-pig ileum. *J Physiol* **471**, 61–86.

Davenport HW (1989). Gastrointestinal physiology, 1895–1975: motility. In *Handbook of Physiology*, Section 6, *Gastrointestinal System*, Part 1, pp. 1–101. American Physiological Society, Bethesda.

Dickens EJ, Edwards FR & Hirst GDS (2001). Selective knockout of intramuscular interstitial cells reveals their role in the generation of slow waves in mouse stomach. *J Physiol* **531**, 827–833.

Dickens EJ, Hirst GDS & Tomita T (1999). Identification of rhythmically active cells in guinea-pig stomach. *J Physiol* **514**, 515–531.

Edwards FR & Hirst GDS (2003). Mathematical description of regenerative potentials recorded from circular smooth muscle of guinea pig antrum. *Am J Physiol* **285**, G661–G670.

Edwards FR & Hirst GDS (2005). An electrical description of the generation of slow waves in the antrum of the guinea pig. *J Physiol* **564**, 213–232.

Goto K, Matsuoka S & Noma A (2004). Two types of spontaneous depolarizations in the interstitial cells freshly prepared from the murine small intestine. *J Physiol* **559**, 411–422.

Hashitani H, Garcia-Londoño AP, Hirst GDS & Edwards FR (2005). Atypical slow waves generated in gastric corpus provide dominant pacemaker activity in guinea pig stomach. *J Physiol* **569**, 459–465.

Hennig GW, Hirst GDS, Park KJ, Smith CB, Sanders KM, Ward SM & Smith TK (2004). Propagation of pacemaker activity in the guinea-pig antrum. *J Physiol* **556**, 585–599.

Hirst GDS & Edwards FR (2001). Generation of slow waves in the antral region of guinea-pig stomach – a stochastic process. *J Physiol* **535**, 165–180.

Hirst GDS, Garcia-Londoño AP & Edwards FR (2006). Propagation of slow waves in the guinea-pig gastric antrum. *J Physiol* **571**, 165–177.

Hodgkin AL & Huxley AF (1952). A quantitative description of membrane current and its application to conduction and excitation in nerve. *J Physiol* **117**, 500–544.

Jack JJB, Noble D & Tsien RW (1983). *Electric Current Flow in Excitable Cells*. Clarendon Press, Oxford, UK.

Jimenez M, Borderies JR, Vergara P, Wang Y-F & Daniels EE (1999). Slow waves in circular muscle of porcine ileum: structural and electrophysiological studies. *Am J Physiol* **276**, G393–G406.

Kito Y, Fukuta H & Suzuki H (2002). Components of pacemaker potentials recorded from the guinea pig stomach antrum. *Pflugers Arch* **445**, 202–217.

Kito Y & Suzuki H (2003). Properties of pacemaker potentials recorded from myenteric interstitial cells of Cajal distributed in the mouse small intestine. *J Physiol* **553**, 803–818.

Kito Y, Ward SM & Sanders KM (2005). Pacemaker potentials generated by interstitial cells of Cajal in the murine intestine. *Am J Physiol* **288**, C710–C720.

Stevens RJ, Publicover NG & Smith TK (1999). Induction and organization of Ca^{2+} waves by enteric neural reflexes. *Nature* **399**, 62–66.

Szurszewski JH (1981). Electrical basis for gastrointestinal motility. In *Physiology of the Gastrointestinal Tract*, ed. Johnson R, pp. 1435–1465. Raven, New York.

Ward SM, Dixon RE, de Foite A & Sanders KM (2004). Voltage-dependent calcium entry underlies propagation of slow waves in canine gastric antrum. *J Physiol* **561**, 793–810.

Acknowledgements

This project was supported by a research grant from the National Health and Medical Research Council of Australia.